

# Preparing Spin Squeezed States via Adaptive Genetic Algorithm

Y. M. Zhao,<sup>1</sup> L. B. Chen,<sup>1</sup> Y. Wang,<sup>1</sup> H. Y. Ma\*,<sup>1</sup> and X. L. Zhao\*\*<sup>1</sup>

<sup>1</sup>*School of Physics, Qingdao University of Technology, 0532, Qingdao, Shandong, China*

(Dated: October 22, 2024)

We introduce a novel strategy employing an adaptive genetic algorithm (GA) for iterative optimization of control sequences to generate quantum nonclassical states. Its efficacy is demonstrated by preparing spin-squeezed states in an open collective spin model governed by a linear control field. Inspired by Darwinian evolution, the algorithm iteratively refines control sequences using crossover, mutation, and elimination strategies, starting from a coherent spin state within a dissipative and dephasing environment. An adaptive parameter adjustment mechanism further enhances optimization. Our approach, compared to constant control schemes, yields a variety of control sequences capable of maintaining squeezing for the collective spin model. Furthermore, the proposed strategy exhibits increased effectiveness in diverse systems, while reservoir thermal excitations are shown to negatively impact control outcomes. We discuss feasible experimental implementations and potential extensions to alternative quantum systems, and the adaptability of the GA module. This research establishes the foundation for utilizing GA-like strategies in controlling quantum systems and achieving desired nonclassical states.

**Keywords:** non-classical state, adaptive genetic algorithm, open quantum system.

## I. INTRODUCTION

Quantum-enhanced metrology has emerged as a cornerstone in the quest for ever-greater precision in measurement, pushing the boundaries of what is achievable using classical systems. Central to this advancement is the development and manipulation of nonclassical quantum states, such as spin-squeezed states, which can surpass the standard quantum limit [1, 2]. Spin squeezing often arises concurrently with entanglement, a consequence of nonlinear interactions within the ensemble [1, 2]. When properly harnessed, this phenomenon has the potential to revolutionize precision measurements by lowering quantum noise in targeted directions of the system's state space. These states reduce quantum uncertainty in specific components of a system's collective spin, enabling unprecedented sensitivity in measurements that are crucial for applications ranging from homodyne interferometers [3–5] to optical atomic clocks [6–8] and magnetometers [9]. However, generating and maintaining highly squeezed states in practical, noisy environments remains a formidable challenge, particularly in systems subject to dissipation and decoherence.

Various approaches have been proposed to achieve spin squeezing [1, 2, 10]. These include quantum non-demolition measurements [11], coherent control [12], and the use of nonlinear interactions in systems such as Bose-Einstein condensates (BECs) [13–15]. While significant progress has been made, there is a continuing need for control methods that not only generate strong squeezing but also maintain coherence over extended periods, especially in the presence of environmental noise.

Machine learning techniques, particularly reinforcement learning (RL), have recently been applied to optimize control strategies in high-dimensional quantum systems [16–18]. These methods excel at exploring complex control landscapes, but they often come with high computational costs and complex hyperparameter tuning, making them less feasible for real-time or large-scale applications. This has spurred interest in alternative optimization strategies that are both scalable and easier to implement. Evolutionary strategies, particularly GAs, offer a promising alternative [19]. GAs simulate the process of natural selection, iteratively refining a population of candidate solutions through mechanisms such as crossover, mutation, and selection. In the context of quantum control, GAs can be particularly advantageous: they offer a flexible and adaptable framework for optimizing control sequences, requiring less detailed prior knowledge of the system's dynamics than gradient-based approaches. Additionally, GAs are well-suited for discrete control problems, such as the optimization of sequences of control pulses [20], where they can explore a vast parameter space with high efficiency.

Building upon these foundations, we propose a novel GA-based optimal control strategy for preparing non-classical spin states in an open environment. Our approach leverages a sequence of square pulses, mimicking bang-bang control [21, 22], to steer the system towards a desired squeezed state. Optimization is achieved through a process mirroring natural selection, where candidate control sequences, encoded as 'individuals', undergo crossover and mutation within 'populations'. Through iterative generations, the fittest individuals are selected, driving the system towards the optimal control solution. We rigorously evaluate the performance of this scheme across a wide range of control parameters, system sizes, and thermal environments, demonstrating its robustness and efficacy. Furthermore, we explore the scalability of the algorithm and its potential applicability to other quantum systems, such as BECs, highlighting its experimental feasibility.

The structure of this paper is as follows: In Section II, we introduce the GA-based optimization framework designed for the preparation of nonclassical quantum states. Section III details the integration of the GA module within the control scheme. In Section IV, we describe the quantum model employed for generating target spin-squeezed states. Section V outlines the procedure for preparing spin-squeezed states in an open collective spin system using the adaptive GA. In Section VI, we evaluate the performance of the proposed method, analyzing the impact of control pulse frequency, control type diversity, system scalability, and thermal excitation. Section VII discusses potential experimental implementations, including the use of BECs and the applicability of this approach to other quantum systems. The adaptability and scalability of the GA module are also discussed. Section VIII summarizes the findings of this study.

## II. CONTROL SCHEME

Inspired by Darwin's theory of evolution [23], genetic algorithms (GAs) have emerged as powerful optimization techniques based on the principles of natural selection. GAs simulate evolutionary processes, subjecting a population of candidate solutions to selection, crossover, and mutation to iteratively generate improved offspring [24], which effectively navigates complex search spaces. This powerful framework has found widespread application across diverse fields, from engineering design to financial modeling, demonstrating its efficacy in tackling complex, non-linear problems [25].

Leveraging the generality of GAs, we propose a control scheme utilizing an adaptive GA to optimize the arrangement of control pulses for the preparation of nonclassical states. We consider a quantum system governed by a general Hamiltonian under the influence of control fields:  $\hat{H} = \hat{H}_0 + \sum_{k=1}^K f_k(t)\hat{H}_k$ , where  $\hat{H}_0$  is the free Hamiltonian and  $K$  denotes the amount of the external control Hamiltonians  $\hat{H}_k$ .  $f_k(t)$  is the amplitude of a time-dependent control field, designed by the GA algorithm. Because of the Heisenberg uncertainty principle, it should be confirmed that  $[\hat{H}_0, \hat{H}_k] \neq 0$ , otherwise, the influence of the control Hamiltonians can be subsumed into the free Hamiltonian.

Figure 1 illustrates the process of obtaining the control sequence by closed-loop emulation, whereas it is implemented in an open-loop control process. The control sequence will steer the system towards a set of states satisfying the desired control target. Our proposed GA framework encodes each individual control sequence within a population that may include the optimal solution. The space of the control sequence explodes exponentially versus the number of control pulses. This results in a huge space for the population.

The versatility of this GA-based approach extends beyond optimizing pulse sequences. It can be readily adapted to optimize the other parameters of the system crucial for achieving the target set. Furthermore, this framework possesses inherent generalizability to be applied to other dynamical systems governed by differential equations. To showcase its efficacy, we demonstrate its application in engineering a collective spin system, illustrating its potential for precise control and manipulation of quantum states.

## III. GENETIC ALGORITHM OPTIMIZES CONTROL SEQUENCE

This section details the logic underpinning our adaptive GA-based optimization strategy for maximizing spin squeezing which can be broadly divided into three key parts:

1. Encoding: GA commences by generating an initial population  $P(x) = \{x_1, x_2, \dots, x_n\}$  of candidate individuals  $x_i$  ( $0 < i \leq n$ ), where  $n$  is the size of the prescribed population. In this control scheme, each individual is encoded as a sequence of discrete control field values that are applied to the spin system over time. The initialized solutions are randomized which ensures diversity within the population, allowing for a broad exploration space of control sequence.

2. Fitness Evaluation: We analyze the evolution of the spin squeezing parameters in a certain time interval, the values are employed to quantify the performance of each control sequence with the function:  $F(x_i) = R(x_i) - R(x)_{min}$ , where  $R(x_i)$  is a measure of performance in GA signifying squeezing degree (final state) after the corresponding control sequence  $x_i$  which is explained in detail later and  $R(x)_{min}$  is the minimum in the population.  $x_i = (\Omega_{1t,i}, \Omega_{2t,i}, \dots, \Omega_{mt,i})$  in the population is one encoded individual, where  $\Omega_{kt,i}$  ( $1 \leq k \leq m$ ) indicates each control pulse in one-time interval, specifically, from  $kt$  to  $(k+1)t$ . We simulate the open collective spin system dynamics under the influence of the control sequence, corresponding to the individual above.

3. Tendentious Selection and Adaptive Genetic Manipulation: To acquire improved solutions as the iteration processes, we implement an elitism strategy based on the roulette wheel selection mechanism: individuals exhibiting higher fitness values, indicative of superior spin squeezing performance, are assigned a higher probability of being selected for the subsequent iteration with a smaller rate of elimination. And the probability of an individual  $x_i$  being selected can be written as:  $p_i = \frac{F(x_i)}{\sum_{l=1}^m F(x_l)}$ , here  $m$  is the total number of individual in the population. This selection

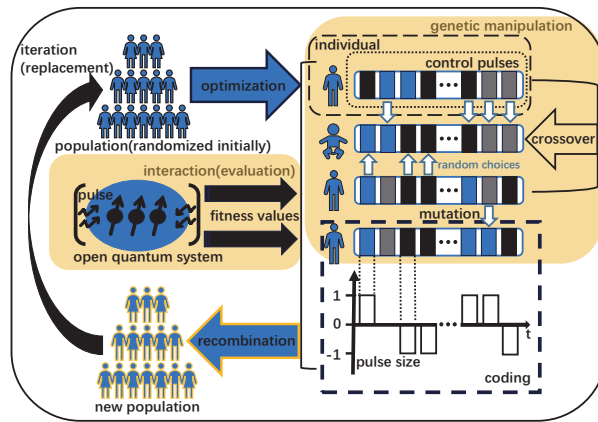


FIG. 1: The GA scheme is used to optimize control pulses for squeezing a spin system in an open quantum system. It starts with a randomly generated population of individuals, each representing a unique control pulse sequence. Individuals undergo crossover and mutation operations to create new offspring. Fitness is evaluated by simulating the open quantum system dynamics under each control pulse, with higher squeezing leading to greater fitness. The GA iteratively selects individuals based on their fitness, promoting the propagation of optimal pulse sequences across generations until the set number of iteration limit is reached.

mechanism, mimicking natural selection, ensures that desirable traits (i.e., control sequences leading to enhanced squeezing) are preferentially propagated through the generations.

To prevent premature convergence and promote the exploration of diverse solutions, we introduce adaptive genetic manipulation on selected individuals, and the ‘adaptive’ is reflected in regulated crossover and mutation rates.

The crossover rate, determining the probability of genetic information exchange between two parent individuals, dynamically adjusts based on their fitness difference in our strategy. This dynamic crossover rate  $c_d$  can be expressed as:

$$c_d = c_s + (1 - c_s) \frac{|F(x_i) - F(x_j)|}{f_h}, \quad (1)$$

where  $c_s$  (0.8 actually) is the minimum mating probability,  $1 - c_s$  guarantees the normalization of the two weighted terms and  $f_h$  (0.5 in the actual algorithm) serves as a scaling factor representing the characteristic fitness difference within the population. So for two parent individuals  $x_i = (\Omega_{1t,i}, \Omega_{2t,i}, \dots, \Omega_{kt,i}, \dots, \Omega_{nt,i})$  and  $x_j = (\Omega_{1t,j}, \Omega_{2t,j}, \dots, \Omega_{kt,j}, \dots, \Omega_{nt,j})$ , their offspring can be:  $x_c = (\Omega_{1t,c}, \Omega_{2t,c}, \dots, \Omega_{kt,c}, \dots, \Omega_{nt,c})$  where each  $\Omega_{kt,c}$  ( $1 \leq k \leq n$ ) ( $\Omega_{kt,c}$  describes the specific control pulse as mentioned in the part of Fitness Evaluation) is acquired with  $\Omega_{kt,c} = \begin{cases} \Omega_{kt,j}, & \text{if } U > c_d \\ \Omega_{kt,i}, & \text{if } U \leq c_d \end{cases}$  and  $U$  is a uniform-distributed random number within (0,1). This formulation ensures that a larger disparity in fitness between parents results in a higher crossover probability, encouraging wider exploration of the potential excellent offsprings.

Conversely, the mutation rate in this task, which governs the introduction of random self-variations in individuals, is progressively reduced with iteration. This dynamic mutation rate  $m_d$  can be formulated as:

$$m_d = m_s \left( 1 - \frac{g_t}{g} \right), \quad (g_t = 1, 2, 3, \dots, g), \quad (2)$$

where  $m_s$  (0.2 in practical situation) is the maximum mutation rate at the initial generation ( $g_t = 1$ ),  $g_t$  is the current generation number, and  $g$  is the total number of generations. This dynamic setting balances exploration in early generations, where diversity is crucial, with the maintenance of the achieved optimization effect as the algorithm converges towards an optimum. Further, maintenance signifies there is less and less probability of variance in population, that is, tendentially exploiting existing solutions to merge.

The algorithm iteratively repeats these steps with a predefined number of iterations, progressively updates the population and searching for control field sequences that decline the spin squeezing parameter furthest.

#### IV. COLLECTIVE SPIN MODEL

To verify the effectiveness of our proposed strategy, we concentrate on an ensemble of  $N$  identical spins, which can be indicated with pseudo spin components  $\hat{J}_\alpha = \frac{1}{2} \sum_{k=1}^N \hat{\sigma}_\alpha^{(k)}$ , ( $\alpha = x, y, z$ ), where  $\hat{\sigma}_\alpha^{(k)}$  is the Pauli operator for the  $k$ -th spin(qubit) [26]. For the symmetric scenario where the operations done on the ensemble have identical impact on all the qubits,  $\hat{J}_x, \hat{J}_y, \hat{J}_z$  fulfill the relationship:  $[\hat{J}_\alpha, \hat{J}_\beta] = i\hbar \epsilon_{\alpha\beta\gamma} \hat{J}_\gamma$ , where  $\epsilon_{\alpha\beta\gamma}$  is the Lévi-Civita symbol. The Hamiltonian can be written as:

$$\hat{H}/\hbar = \kappa \hat{J}_z^2 + \Omega_x(t) \hat{J}_x, \quad (3)$$

here the first term is the nonlinear interaction in the one-axis twisting (OAT)-type spin squeezing [10] which can provide the resource for quantum-enhanced metrology [2, 10].  $\kappa$  is the atomic interaction strength which is assumed as the unit ( $\kappa = 1$ ) in this work. It experimentally depends on the scattering lengths between the particles and the condensate density [15] and  $\Omega_x(t)$  is the strength of the transverse external field.

The collective spin dynamics can be transformed to its dual bosonic representation through Schwinger's transformation methodology:  $\hat{J}_z = \frac{1}{2}(\hat{a}^\dagger \hat{a} - \hat{b}^\dagger \hat{b})$ ,  $\hat{J}_+ = \hat{a}^\dagger \hat{b}$  and  $\hat{J}_- = (\hat{J}_+)^\dagger$ , where  $\hat{a}(\hat{a}^\dagger)$  and  $\hat{b}(\hat{b}^\dagger)$  are the two annihilation (creation) operators of two boson modes. In this perspective, the assignment of one mode to represent the spin-up state and the other to signify the spin-down state allows  $\hat{J}_z$  to encapsulate the disparity in population between the two modes within the framework of a Ramsey interferometer [2, 3, 10, 27]. Analogous to a linear beam splitter in interferometry, the coupling Hamiltonian term  $\hat{J}_x$  effects a rotation of the collective spin by an angle  $\theta = \int_{t_0}^{t_0+\Delta t} \Omega(t) dt$  around the  $x$ -axis over a time interval  $\Delta t$ .

In distinction from the utilization of a static control [12] and periodic control [28], the present proposal employs a genetic algorithm optimizing the external control field  $\Omega_x(t)$  as a sequence of rectangular pulses, to prepare nonclassical states. The pulsed control is operationally analogous to a series of linear beam splitters in an interferometer, manipulating the spin system [14, 15]. The linear control Hamiltonian's capability to steer the spin system arises from the non-commutability:  $[\hat{J}_z^2, \hat{J}_x] = i(\hat{J}_y \hat{J}_z + \hat{J}_z \hat{J}_y) \neq 0$ .

The degree of spin squeezing can be effectively quantified using parameters structured from the expectation values of collective spin operators, as detailed in seminal works [1, 2]. Achieving variances below the standard quantum limit signifies the onset of spin squeezing, rendering the system suitable for precision metrology by virtue of amplified sensitivity in the spin components perpendicular to the mean-spin direction. A crucial parameter for quantifying spin squeezing is

the minimum squeezing parameter, defined as:  $\xi_\perp^2 = \frac{N \min(\Delta \hat{J}_{\vec{n}_\perp}^2)}{|\langle \hat{J}_o \rangle|^2} = \frac{N \left[ \langle \hat{J}_{\vec{n}_1}^2 + \hat{J}_{\vec{n}_2}^2 \rangle - \sqrt{\langle \hat{J}_{\vec{n}_1}^2 - \hat{J}_{\vec{n}_2}^2 \rangle^2 + \langle [\hat{J}_{\vec{n}_1}, \hat{J}_{\vec{n}_2}]_+ \rangle^2} \right]}{2|\langle \hat{J}_o \rangle|^2}$ , where  $\hat{J}_{\vec{n}_i}$  is the collective spin component along the unit vector  $\vec{n}_i$  ( $i = 1, 2$ ), defined as  $\hat{J}_{\vec{n}_i} = (\hat{J}_x, \hat{J}_y, \hat{J}_z) \cdot \vec{n}_i$ , ( $i = 1, 2$ ). The specific directions are given by  $\vec{n}_1 = (-\sin \phi, \cos \phi, 0)$  and  $\vec{n}_2 = (\cos \theta \cos \phi, \cos \theta \sin \phi, -\sin \theta)$ . The collective spin operator along the mean spin direction is defined as  $\hat{J}_o = (\hat{J}_x, \hat{J}_y, \hat{J}_z) \cdot (\sin \theta \cos \phi, \sin \theta \sin \phi, \cos \theta)$ , with  $\theta$  and  $\phi$  representing the polar and azimuth angles of the mean spin vector, respectively. These angles are determined by  $\theta = \arccos(\frac{\langle \hat{J}_z \rangle}{|\hat{J}|})$  and  $\phi = \text{sign}(\langle \hat{J}_y \rangle) \arccos(\frac{\langle \hat{J}_x \rangle}{|\hat{J}| \sin \theta})$ , where  $|\hat{J}| = \sqrt{\langle \hat{J}_x \rangle^2 + \langle \hat{J}_y \rangle^2 + \langle \hat{J}_z \rangle^2}$  is the magnitude of the mean spin vector [1, 2, 29]. The direction  $\vec{n}_\perp$  corresponding to the minimum spin variance is given by  $\vec{n}_\perp = \vec{n}_1 \cos \varphi + \vec{n}_2 \sin \varphi$ , where the angle  $\varphi$  corresponds to the best direction with the lowest squeezing parameter, satisfying

$$\varphi = \begin{cases} \frac{1}{2} \arccos\left(\frac{-A}{\sqrt{A^2+B^2}}\right) & \text{if } B \leq 0, \\ \pi - \frac{1}{2} \arccos\left(\frac{-A}{\sqrt{A^2+B^2}}\right) & \text{if } B > 0. \end{cases} \quad (4)$$

Here,  $A \equiv \langle \hat{J}_{\vec{n}_1}^2 - \hat{J}_{\vec{n}_2}^2 \rangle$ ,  $B \equiv \langle [\hat{J}_{\vec{n}_1}, \hat{J}_{\vec{n}_2}]_+ \rangle$  are defined for brevity.

In this control scheme, we employ the following definition

$$\xi_z^2 = \frac{4\Delta \hat{J}_z^2}{N}, \quad (5)$$

as the squeezing parameter, where  $\Delta \hat{J}_z^2 = \langle \hat{J}_z^2 \rangle - \langle \hat{J}_z \rangle^2$  indicates the spin squeezing in the  $z$ -direction [1].

For the GA optimization scheme, the performance function is calculated by:

$$\begin{aligned} R_{x_i} &= P_{final} R_{final} + P_{process} \langle R_{process} \rangle, \\ &= P_{final} R(\Omega_{mt,i}) + P_{process} \frac{\sum_{q=1}^{m-1} R(\Omega_{qt,i})}{m-1}, \end{aligned} \quad (6)$$

where

$$R_{final} = \frac{1}{\xi_{Z,final}^2} = \frac{N}{4\Delta\hat{J}_{z,final}^2} \quad (7)$$

is the performance score corresponding to the final state after the application of the entire control sequence, while  $\langle R_{process} \rangle$  is the mean value of the performance scores corresponding to the sampling points(after each pulse is applied) in the control process calculated with the same formula (Eq. 7).  $P_{final}$  and  $P_{process}$  are two constants(0.8 and 0.2 in simulation) for the entire training session, representing the contribution weights of the degree of final state squeezing and the average degree of process states to the evaluation of the quality of one control sequence.  $R_{x_i}$  corresponding to each individual is an important basis for calculating individual fitness at the population level, as the evaluated fitness value is defined with the difference between individual performance value and the smallest performance value in the population. Subsequently, compared to using the reverse of  $\xi_1^2$  with variable  $\theta$  and  $\phi$ , the choice of  $\xi_Z^2$  possesses a more direct physical interpretation since  $\hat{J}_z = \frac{1}{2}(a^\dagger a - b^\dagger b) = \frac{1}{2}(\hat{N}_a - \hat{N}_b)$  indicates the population imbalance between the two modes as well as the phase difference between two detectors within the Ramsey interferometer [2, 3, 10], while  $\hat{N}_a$  and  $\hat{N}_b$  signify the atom number of two modes.

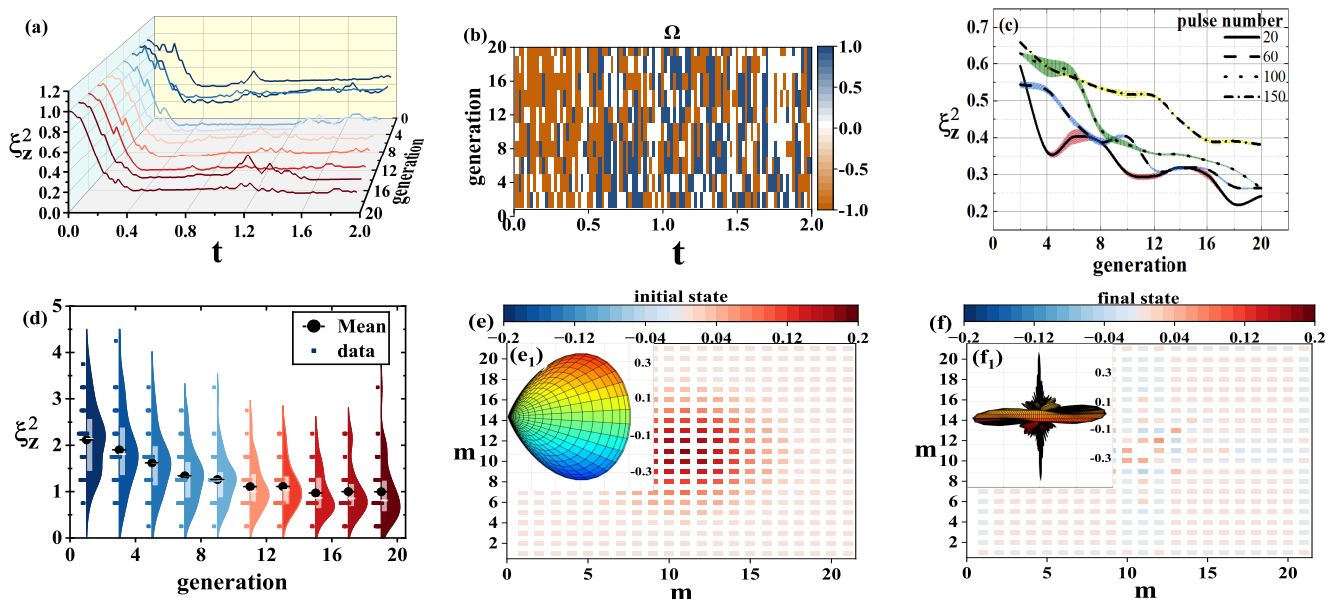


FIG. 2: (a) Evolution of the spin squeezing parameter while 100 rectangular pulses are taken across each evolution time interval  $[0, 2]$  and a total of 20 consecutive training rounds are shown with 10 iteration curves (one curve is displayed every two generations). (b) Schematic representation of the three-level ( $\Omega(t) = 1, 0, -1$ ) square control pulses used in (a). (c) The evolution of average spin squeezing parameter with different pulse numbers and corresponding variance of squeezed state at  $t = 2$  during iterations. (d) Evolutionary trend of the statistical distribution, average, and median of final-state squeezing parameter values for individuals within uniform-sampled 10 generations, and each ‘violin’ pattern corresponds to one generation as well as to one population. Solid black balls represent the mean, and white bars represent the median. (e) The real part of the density matrix of the initial CSS and  $(e_1)$  is the Wigner representation of it. (f) The real part of the matrix of the spin-squeezed state at  $t = 2$  and  $(f_1)$  is its corresponding Wigner representation.  $\gamma/\kappa = 0.001$  and  $\gamma_z/\kappa = 0.001$  in these results.

## V. PROCEDURE TO PREPARE SPIN-SQUEEZED STATES USING GENETIC ALGORITHM

The procedure for generating spin-squeezed states encompasses two principal stages: initially, the establishment of a spin coherent state, followed by the application of a genetically optimized control sequence, to achieve the desired spin-squeezing.

### A. Initial coherent spin state

A collection of  $N$  identical two-level atoms, each aligned in the same direction, is aptly represented by SU(2) coherent spin state (CSS), which can be articulated as the projection of a coherent state onto Dicke states  $|j, m\rangle$ , reads

$$\begin{aligned} |\eta\rangle &\equiv |\theta, \phi\rangle \\ &= (1 + |\eta|^2)^{-j} \sum_{m=-j}^j \binom{2j}{j+m}^{1/2} \eta^{j+m} |j, m\rangle, \\ &= \exp(\eta \hat{J}_+) \exp\left[\ln(1 + |\eta|^2) \hat{J}_z\right] \exp(-\eta^* \hat{J}_-) |j, j\rangle, \end{aligned} \quad (8)$$

where  $\eta = -\tan\frac{\theta}{2} \exp(-i\phi) \in \mathbb{C}$ ,  $|j, m\rangle$  are the eigenstates of  $\hat{J}_x$  with eigenvalue  $m$ , satisfying the equations:  $\hat{J}^2|j, m\rangle = j(j+1)\hbar^2|j, m\rangle$  and  $\hat{J}_z|j, m\rangle = m\hbar|j, m\rangle$  ( $\hbar=1$  in numerical calculations);  $|j, j\rangle \equiv \bigotimes_{l=1}^N |0\rangle_l$  represents a state with all the spins polarized in the z-direction. This overcomplete state is most similar to the classical one with  $\theta$  and  $\phi$  being the azimuth angles for longitude and latitude, respectively. The quantum state can be generated by the effect of rotation operator  $\hat{R}(\theta, \phi) = e^{-i\theta\hat{J}_{\vec{n}}} = e^{i\theta(\hat{J}_z \sin\phi - \hat{J}_y \cos\phi)}$  [1], where  $\vec{n} = (-\sin\phi, \cos\phi, 0)$  on the eigenstate of  $\hat{J}_z$  with the applicable Husimi Q-function:

$$Q(\theta, \phi) = \langle \theta, \phi | \rho | \theta, \phi \rangle \quad (9)$$

visualizing the probability density of quantum state having coordinates  $\theta$  and  $\phi$  in the phase space,  $\rho$  is the density matrix of the collective spin system in the reservoir. It can also be represented by the Wigner distribution which is calculated in the collective model as  $W_{jm}(\theta, \varphi) = \sum_{k=0}^{2j} Y_{k0}(\theta, \varphi) (-1)^{j-m} \sqrt{2k+1} \times \begin{bmatrix} j & k & j \\ -m & 0 & m \end{bmatrix}^*$ , where  $\begin{bmatrix} j & k & j \\ -m & 0 & m \end{bmatrix}^*$  is the Wigner 3j symbol [30] and  $Y_{k0}$  is the spherical harmonic. Furthermore, the CSS can be prepared by applying  $\pi/2$  pulses to a BEC with  $N$  atoms in the internal ground state [13–15], where  $\langle \hat{J}_x \rangle = N/2 = J$  and  $\langle \hat{J}_y \rangle = \langle \hat{J}_z \rangle = 0$  and the internal wave function  $|\Psi\rangle$  of the BEC is thus written by:  $|\Psi(t=0)\rangle = \frac{1}{\sqrt{2^N N!}} (a^\dagger + b^\dagger)^N |\text{vac}\rangle$ , where  $|\text{vac}\rangle$  is the vacuum state. Starting with a CSS aligned along the  $x$ -axis and exhibiting isotropic fluctuations in its spin components, the application of  $\hat{J}_z^2$  induces a shear, transforming the state into a spin-squeezed state with reduced variance in  $z$  direction. This results in a state that surpasses the standard quantum limit, thereby enhancing metrological measurement sensitivity along the direction of squeezing [31]. The direction of squeezing is dynamically adjusted by the action of  $\Omega(t)\hat{J}_x$ , which is initially randomized and subsequently refined through optimization by the GA as previously described.

### B. Prepare spin-squeezed states by GA-optimized pulses

Preserving the integrity of quantum states against the detrimental effects of decoherence, induced by inevitable interactions with the environment, is a formidable challenge in quantum technologies. Effective quantum control strategies are thus crucial for mitigating decoherence and safeguarding the delicate quantum resources that underpin coherent quantum operations. This study investigates the impact of two prominent decoherence channels, namely, superradiant damping and dephasing, both notorious for their capacity to erode quantum coherence and compromise quantum information processing. The temporal evolution of the collective spin dynamics is rigorously described by the Lindblad master equation, formulated as:

$$\dot{\rho} = -i[\hat{H}, \rho] + \gamma(n_{th} + 1)\mathcal{L}_{\hat{J}_-}\rho + \gamma n_{th}\mathcal{L}_{\hat{J}_+}\rho + \gamma_z\mathcal{L}_{\hat{J}_z}\rho, \quad (10)$$

where  $\mathcal{L}\hat{X}\rho = 2\hat{X}^\dagger\rho\hat{X} - \hat{X}\hat{X}^\dagger\rho - \rho\hat{X}\hat{X}^\dagger$ ,  $\rho$  is the density matrix for the controlled system. Here,  $\gamma$  denotes the decay rate,  $\gamma_z$  represents the dephasing rate, and  $n_{th}$  signifies the average thermal photon number. Unlike conventional quantum Lyapunov control methods, which focus on minimizing the distance between eigenstates, specifically, increasing the inner product between current state and target state [32], our approach leverages a GA to optimize the control sequence  $\Omega(t)$  within the Hamiltonian Eq. 3, thereby guiding the system's evolution under the Lindblad master equation.

Our approach employs a GA to identify optimal sequences of control pulses for driving a spin system toward a desired spin-squeezed state. The algorithm explores a population of candidate control sequences, where each individual within

this population represents a sequence of square pulses. We quantify the effectiveness of each control sequence (Eq. 6) by simulating the evolution of the spin system under its influence, according to the master equation Eq. 10. The degree of spin squeezing achieved at the end of the evolution serves as a main fitness measure (Eq. 6), with higher fitness values assigned to sequences yielding stronger squeezing (Eq. 7).

This iterative optimization process proceeds as follows. Each control sequence is encoded and then evaluated by quantifying the resulting spin squeezing after the simulation of the system's dynamics. Based on these fitness evaluations, a selection process preferentially propagates higher-fitness sequences to subsequent generations, mimicking natural selection. To further enhance exploration and prevent convergence to local optima, crossover and mutation operators are introduced, introducing randomness into the offspring generation. Respectively, crossover facilitates the combination of beneficial traits from different parent sequences, while mutation stochastically explores new regions of the control parameter space.

It is crucial to emphasize that while the optimization process utilizes a closed-loop simulation, the resulting control strategy is implemented in an open-loop manner. This distinction is critical for practical applications. During the optimization, once the optimal control sequence, such as the  $\Omega_x(t)$  defined in Eq. 3, is identified, it is applied in a single, uninterrupted open-loop control process. This avoids wavefunction collapse associated with continuous measurements during the control implementation, preserving the coherence necessary for achieving the desired spin-squeezed state.

## VI. CONTROL RESULTS

The control protocol, illustrated in Fig. 2, divides the time interval  $[0, 2]$  into a variable number of segments. Square control pulses are applied at the boundaries between the adjacent time segments and sustained until the subsequent boundary. The control pulse sequences are generated randomly in groups at the beginning and optimized and renewed by GA. The GA optimizes these pulse sequences over 20 generations and every 2 generations of the evolution for the squeezing parameter are illustrated in Fig. 2 (a). It can be seen that, at the first stage of the training, the GA has already found the effective control sequence, resulting in the downward trend of  $\xi_Z^2$ . As the training proceeds, even after a small number of iterations, the GA can find a sequence of square pulses inducing an optimal performance of squeezing, however, it does not show a further improvement in subsequent iterations before the end. Fig. 2 (b) illustrates the timing of the corresponding square wave control pulses. In Fig. 2 (c), when the frequency of pulse application is higher, the squeezing effect of the final state of each generation changes more gradually with the iteration, but the overall squeezing effect is poor. Corresponding to Fig. 2 (d), the statistical distribution of final-state squeezing parameters for individuals within the evolving population reveals a clear trend: as the optimization control progresses, the proportion of relatively advantageous individuals (characterized by  $\xi_Z^2 < 1$ ) steadily increases. These results validate the GA optimization strategy for enhancing control pulse performance.

It's worth mentioning that the distribution of squeezing parameter adheres to the principles of Kernel Density Estimation (KDE), a non-parametric statistical method employed to estimate the probability density function (PDF) of a dataset and derive a smooth representation of the underlying distribution, which offers a robust alternative to parametric methods, as it avoids imposing assumptions about the specific form of the distribution (e.g., Gaussian, exponential). The kernel density estimator's formula is given by  $\hat{f}_h(x) = \frac{1}{nh} \sum_{i=1}^n K\left(\frac{x-x_i}{h}\right)$ , where  $x_1, x_2, \dots, x_n$  are acquired samples from an unacquainted distribution,  $n$  is the sample size,  $h$  is the bandwidth and  $K(\cdot)$  is the kernel function [33]. Instead, KDE leverages  $K(\cdot)$  to smoothly distribute the probability mass associated with each data point, resulting in a continuous and differentiable estimate of the PDF. Consequently, both the average (black dots with black horizontal bars) and median (white horizontal bar) squeezing coefficients exhibit a decline. However, due to the intentional preservation of a degree of exploratory freedom (mutation rate  $m_d \geq 0$ ) and the finite duration of the iterative process, it is not possible to achieve effective control for all individuals within the population during the tested number of iterations.

Furthermore, Fig. 2 ( $e_1$ ) and ( $f_1$ ) utilize the Wigner function to visualize the initial coherent spin state and final spin-squeezed state at the time  $t = 2$ . The irregular folds in Wigner-like function is relevant to non-classical effect which leads to interesting interference effects [34]. This provides insight into the evolution of the quantum state under control. To show the squeezing process more vividly, a movie of the squeezing process is shown by the Husimi function in [35]. We investigate the impact of pulse frequency on control effectiveness by discretizing the time interval  $[0, 2]$  into different numbers of segments (more segments corresponds to higher frequency). Fig. 3(a) shows that higher frequencies lead to lower variance in the squeezing parameter but a slower decrease of mean value at early steps. This reveals a trade-off between control performance and experimental complexity: if we pursue a more stable control effect on the squeezing parameter, more pulses are needed in a certain time period, which is more demanding for the experimental device. Because the genetic algorithm is essentially the optimization of the sequence, it is not limited by the sequence length, and the sequence length in this task only depends on the number of controls (the number of

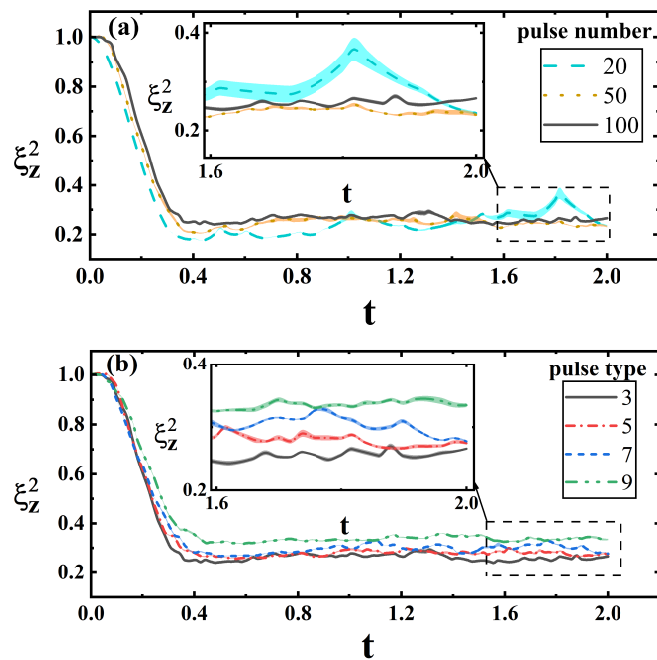


FIG. 3: (a) Mean evolution of the last iteration sample of  $\xi_Z^2$  in 5 repetitions every 30 generations. The shaded regions indicate the variance for different frequencies of applying rectangular pulses. Control time interval  $[0, 2]$  is divided into the number of specific segments at which the square pulses with three levels ( $\Omega(t) = 1, 0, -1$ ) are applied. Samples were all obtained from the final generation results of each training session. (b) Evolution of the spin squeezing parameter for different numbers of pulse gears when 100 total pulses are applied, and the correspondence between the number of pulses and their intensity is as follows:  $\{\Omega(t)\} = \{(1, 0, -1) | \text{actions} = 3\}$ ,  $\{(1, 0.5, 0, -0.5, -1) | \text{actions} = 5\}$ ,  $\{(1, 0.67, 0.33, 0, -0.33, -0.67, -1) | \text{actions} = 7\}$ ,  $\{(1, 0.75, 0.5, 0.25, 0, -0.25, -0.5, -0.75, -1) | \text{actions} = 9\}$ .

time segments) in the total time scale, which can theoretically optimize the high-frequency-varying control sequence.

We also investigate the influence of the number of pulse gears on control performance. As shown in Fig. 3(b), there is an obvious advantage for fewer control types with the same maximum control amplitude in this control, which conclusion is different from the previous conclusion of using reinforcement learning for control. The reason may lie in the following: with the number  $p$  of control pulses remaining constant in total time  $[0, 2]$ , when the number of control types increases from  $q$  to  $q + d$ , the search space for the optimal control sequence explored by GA expands by  $\left(\frac{q+d}{q}\right)^p$ . Consequently, within the same limited number of iterations, the probability of finding an optimal control sequence becomes smaller.

The generalizability of our approach is investigated by applying it to collective spin models with different total spin number ( $N = 2J$ ). Figure 4 presents the control results for different  $N$ s. The results show that the larger the  $N$ , the faster the compression parameter drops at the beginning, however, the corresponding squeezing parameter rebounds more strongly at the final time cut-off. This observation indicates that a lessened ensemble of spins benefits enhancing the precision of quantum metrology. Interestingly, this conclusion is also different from previous observations of using reinforcement learning [28], but the mechanism of occurrence is unknown.

The environmental temperature was assumed to be zero in the previous results. To investigate the robustness of the proposed control scheme, it is essential to examine how temperature affects the control outcomes. Since the temperature is positively correlated with the average number of thermal excitations in the reservoir, denoted by  $n_{th} = \frac{1}{\exp(\hbar\omega/k_B T) - 1}$  [36], it indicates the strength of the decoherence. Here,  $T$  is the temperature of the reservoir. As shown in Fig. 5, a gradual increase in thermal excitations reduces the effectiveness of the control strategy.

Substantially, in the system we analyze, the applied coherent pulses interfere with the energy dissipation and decoherence that would otherwise drive the quantum system to its ground state. This competition establishes a dynamic equilibrium, enabling stable maintenance of the squeezing parameter.



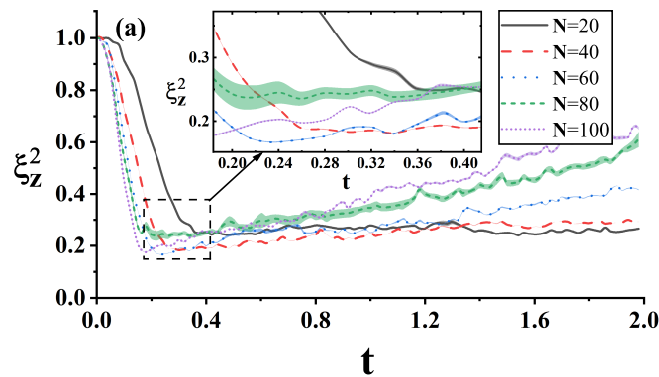


FIG. 4: Evolutions for the last iteration of  $\xi_Z^2$  every 30 generations for different sizes of the collective spin system  $N = 2J$  under three-type ( $\Omega(t) = 1, 0, -1$ ) control. The error zone corresponding to variance is calculated by five repetitions. The samples are picked in the same manner as those in Fig. 3 (a) and number of segments is 100.

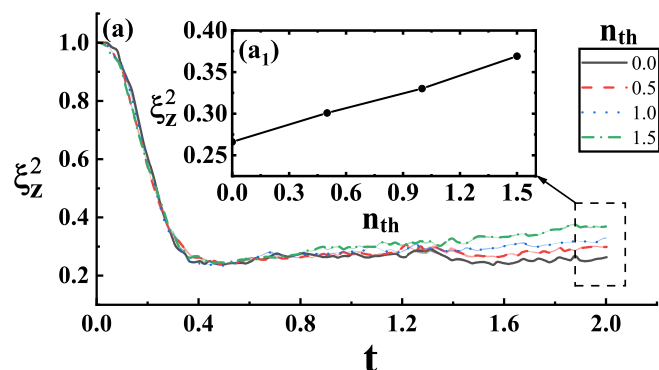


FIG. 5: The average evolutions of the last iteration of  $\xi_Z^2$  in 5 repetitions every 30 generations with variance for different thermal excitations: the average number of photons for a mode with frequency  $\omega$  in the reservoir. The samples are picked in the same manner as those shown in Fig. 4. The subgraph shows the squeezing parameter versus average thermal excitation at  $t = 2$ .

## VII. DISCUSSIONS

### A. Feasible experiments

Atomic BECs offer a compelling platform for realizing this proposed control scheme, where interactions between atoms can be finely tuned, making them ideal candidates for demonstrating spin squeezing and quantum control. In these experiments, the condensate ensemble can be effectively described by the Hamiltonian Eq. 3 [15, 37–39]. Specifically, the experimental realization of our scheme can be based on the hyperfine states of atoms in a BEC, which can naturally map onto the spin-up and spin-down states of our model.

The nonlinear interaction term  $\hat{J}_z^2$  is crucial because it can be directly controlled by adjusting the normalized density overlap of the two BEC components. This overlap, in turn, can be precisely tuned using Feshbach resonances [40, 41], a technique successfully employed in various experiments exploring spinor BEC dynamics [42, 43]. Furthermore, The time-dependent control field, represented by the Rabi frequency  $\Omega(t)$ , can be readily implemented with  $\pi/2$  microwave pulses. These pulses couple the near-resonant two-photon hyperfine states of a  $^{87}\text{Rb}$  or  $^{23}\text{Na}$  BEC confined in an optical lattice [15, 37, 38, 44–46]. Importantly, our proposed scheme requires only minimal modification of existing experimental setups; only a carefully timed sequence of Rabi pulses needs to be implemented. This high degree of compatibility with current BEC experiments makes our approach a promising avenue for realizing optimized spin squeezing in the near future.

## B. Diversity of application

Optimizing control in systems with continuous variables presents a distinct challenge compared to discrete systems, due to the vastness of the control landscape and the complexity of feedback mechanisms. In such systems, control fields are continuous functions of time, and finding the optimal time-dependent control requires exploring a vast parameter space. Despite the added difficulty, and even in the presence of noise from measurement feedback, GA has proven effective in tackling continuous-space control problems, such as its viability of continuously adapting the robot controllers [47]. As noted in various fields, GAs can also handle the optimization of multi-dimensional functions efficiently by employing real-valued encodings and specialized operators. This capability makes GAs highly applicable to continuous quantum control tasks, such as steering the open-ended evolution of quantum states.

Furthermore, the inherent per-particle symmetry of our control scheme within the interferometer naturally extends its applicability to bosonic systems. In the large-particle-number limit( $N$ ), the collective spin model can be mapped onto a bosonic model via the Holstein-Primakoff transformation:  $\hat{J}_z = N/2 - \hat{a}^\dagger \hat{a} \simeq N/2$ ,  $\hat{J}_x = \hbar \frac{\sqrt{2J - \hat{a}^\dagger \hat{a}} + \hat{a}^\dagger \sqrt{2J - \hat{a}^\dagger \hat{a}}}{2}$  and  $\hat{J}_y = \hbar \frac{\sqrt{2J - \hat{a}^\dagger \hat{a}} - \hat{a}^\dagger \sqrt{2J - \hat{a}^\dagger \hat{a}}}{2i}$  where  $\hat{a}$  ( $\hat{a}^\dagger$ ) denotes the bosonic annihilation (creation) operator [48]. This mapping facilitates the direct application of our control strategy to engineer quantum resources in bosonic systems, further showcasing the broad scope of our approach.

## C. Replaceability of the genetic algorithm module

GA is used here to implement the control scheme, it can be readily replaced with alternative optimization algorithms possessing similar learning capabilities without altering the fundamental structure of our approach.

Several promising candidates exist for substituting the GA, each with its own strengths and limitations. These include Particle Swarm Optimization [49], Ant Colony Optimization(ACO) [50], and Firefly Algorithm(FA) [51], among others. In ACO, the pathfinding process of each ‘ant’ can be viewed as searching for the optimal arrangement of a sequence and the algorithm mimics the foraging behavior of ants to find the best sequence. In FA, each ‘firefly’ represents a potential sequence solution, and the ‘brightness’ of a firefly represents the quality of the solution. The algorithm simulates the flashing and mutual attraction behavior of fireflies to find the optimal sequence. Analogous to our application of GA for optimizing time-varying control fields, all these algorithms applicable to sequence optimization may theoretically be employed to design the arrangement of time-varying control pulses. The optimal choice of optimization algorithm will likely depend on specific features of the control problem, such as the dimensionality of the search space, the complexity of the fitness landscape, and computational resource constraints.

The broader principle underlying our control scheme is the utilization of a feedback loop to guide the dynamical evolution of a quantum system toward a desired target state. The optimization module, whether it be a GA or an alternative algorithm, serves as a tool to efficiently navigate the control landscape and identify the most effective pathways for achieving this goal. The key advantage of these optimization techniques lies in their ability to leverage existing knowledge of high-performing solutions while simultaneously exploring new possibilities. This balance of exploitation and exploration allows for the discovery of control strategies that may not be readily apparent through intuitive design or brute-force search methods. By framing the control problem as an optimization task, we open the door to a powerful and versatile toolkit for manipulating quantum systems with high fidelity and precision.

## VIII. CONCLUSION

We pioneered the application of GA, traditionally used for spatial sequence optimization, to the design of time-dependent control fields, successfully generating target spin-squeezed states in an open system. Iterative optimization of the control pulse sequences enhances the generation of these states. That is, iteration-adaptive crossover and mutation rate improve the optimization efficiency, as early iterations focus on exploration, but gradually tend to be conservative. Corresponding to this task, a good squeezing effect (squeezing parameter of the state drops to approach the Heisenberg limit and the process fluctuates less) is achieved in early generations and maintained in subsequent iterations. Pulses with higher frequency generally improve performance and stability, while increasing the complexity of the control types (i.e., more choices of pluses) can negatively impact the results. The framework’s scalability satisfies application to larger systems, and the thermal excitations degrade control performance. This control proposal is readily implementable within existing experimental setups for atomic Bose-Einstein condensates. Furthermore, the paradigm can be extended to other quantum systems. Its universality is further highlighted by the possibility of replacing the genetic algorithm with alternative optimization schemes.

## IX. ACKNOWLEDGEMENTS

X. L. Zhao thanks the Natural Science Foundation of Shandong Province, China, No.ZR2020QA078, No.ZR2023MD064, and National Natural Science Foundation of China, No.12005110, No.12074206. Joint Fund of Natural Science Foundation of Shandong Province, No.ZR2022LLZ012. Key Research and Development Program of Shandong Province, China, No.2023CXGC010901.

- 
- [1] J. Ma, X. G. Wang, C. P. Sun, and F. Nori, *Physics Reports* **509**, 89 (2011).
- [2] L. Pezzè, A. Smerzi, M. K. Oberthaler, R. Schmied, and P. Treutlein, *Rev. Mod. Phys.* **90**, 035005 (2018).
- [3] D. J. Wineland, J. J. Bollinger, W. M. Itano, F. L. Moore, and D. J. Heinzen, *Phys. Rev. A* **46**, R6797 (1992).
- [4] D. J. Wineland, J. J. Bollinger, W. M. Itano, and D. J. Heinzen, *Phys. Rev. A* **50**, 67 (1994).
- [5] O. Hosten, N. J. Engelsen, R. Krishnakumar, and M. A. Kasevich, *Nature* **529**, 505 (2016).
- [6] W. J. Eckner, N. Darkwah Oppong, A. Cao, W. Y. Aaron, R. M. William, M. R. John, Y. Jun, and M. K. Adam, *Nature* **621**, 734 (2023).
- [7] J. M. Robinson, M. Miklos, Y. M. Tso, C. J. Kennedy, T. Bothwell, D. Kedar, J. K. Thompson, and J. Ye, *Nature Physics* **20**, 208 (2024).
- [8] E. Pedrozo-Peñañafiel, S. Colombo, C. Shu, A. F. Adiyatullin, Z. Li, E. Mendez, B. Braverman, A. Kawasaki, D. Akamatsu, Y. Xiao, and V. Vuletić, *Nature* **588**, 414 (2020).
- [9] R. J. Sewell, M. Koschorreck, M. Napolitano, B. Dubost, N. Behbood, and M. W. Mitchell, *Phys. Rev. Lett.* **109**, 253605 (2012).
- [10] M. Kitagawa, and M. Ueda, *Phys. Rev. A* **47**, 5138 (1993).
- [11] A. Kuzmich, N. P. Bigelow, and L. Mandel, *Europhys. Lett.* **42**, 481 (1998).
- [12] C. K. Law, H. T. Ng, and P. T. Leung, *Phys. Rev. A* **63**, 055601 (2001).
- [13] A. Sørensen, L. M. Duan, J. L. Cirac, and P. Zoller, *Nature* **409**, 63 (2001).
- [14] C. Gross, T. Zibold, E. Nicklas, J. Estève, and M. K. Oberthaler, *Nature* **464**, 1165(2010).
- [15] M. F. Riedel, P. Böhi, Y. Li, T. W. Hänsch, A. Sinatra, and P. Treutlein, *Nature* **464**, 1170(2010).
- [16] K. P. Murphy, *Machine Learning: A Probabilistic Perspective*, MIT Press (2012).
- [17] R. S. Sutton, and A. G. Barto, *Reinforcement learning: An introduction*, MIT Press (2018).
- [18] J. Biamonte, P. Wittek, N. Pancotti, P. Rebentrost, N. Wiebe, and S. Lloyd, *Nature* **549**, 195 (2017).
- [19] T. Salimans, J. Ho, Xi Chen, S. Sidor, and I. Sutskever, arXiv:1703.03864(2017).
- [20] P. J. Fleming, and R. C. Purshouse, *Control engineering practice* **10**, 1223 (2002).
- [21] L. Viola, and S. Lloyd, *Phys. Rev. A* **58**, 2733 (1998).
- [22] S. C. Hou, M. A. Khan, X. X. Yi, Daoyi Dong, and Ian R. Petersen, *Phys. Rev. A* **86**, 022321 (2012).
- [23] C. Darwin, London: John Murray (1859).
- [24] J. H. Holland, MIT press (1992).
- [25] D. E. Goldberg, and J. Richardson, *Genetic algorithms and their applications: Proceedings of the Second International Conference on Genetic Algorithms.* **4149** (1987).
- [26] F. T. Arecchi, E. Courtens, R. Gilmore, and H. Thomas, *Phys. Rev. A* **6**, 2211 (1972).
- [27] L. G. Biedertarn, and J. C. Louck, *Angular Momentum in Quantum Physics Theory and Application*, (Addison-Wesley, Reading, MA, 1981).
- [28] X. L. Zhao, Y. M. Zhao, M. Li, T. T. Li, Q. Liu, S. Guo, and X. X. Yi, *Ann. Phys. (Berlin)* **536**, 2400056 (2024).
- [29] L. Song, X. Wang, D. Yan, and Z. Zong, *J. Phys. B: At. Mol. Opt. Phys.* **39** 559(2006).
- [30] G. S. Agarwal, *Phys. Rev. A* **24**, 2889 (1981).
- [31] V. Giovannetti, S. Lloyd, and L. Maccone, *Science* **306**, 1330 (2004).
- [32] X. L. Zhao, Y. L. Ma, H. Y. Ma, T. H. Qiu, and X. X. Yi, *Physics Letters A* **425**, 127874 (2022).
- [33] A. W. Bowman, and A. Azzalini, New York: Oxford University Press **18** (1997).
- [34] D. Harland, M. J. Everitt, K. Nemoto, T. Tilma, and T. P. Spiller, *Phys. Rev. A* **86**, 062117 (2012).
- [35] A movie shows the squeezing process by Husimi function.
- [36] A. Rivas, and S. F. Huelga, Berlin: Springer **10**, 978-3 (2012).
- [37] Y. Q. Zou, L. N. Wu, Q. Liu, X. Y. Luo, S. F. Guo, J. H. Cao, M. K. Tey, and L. You, *Proceedings of the National Academy of Sciences* **115**, 6381 (2018).
- [38] C. Gross, T. Zibold, E. Nicklas, J. Estève, and M. K. Oberthaler, *Nature* **464**, 1165 (2010).
- [39] W. Müssel, H. Strobel, D. Linnemann, D. B. Hume, and M. K. Oberthaler, *Phys. Rev. Lett.* **113**, 103004 (2014).
- [40] S. Inouye, M. R. Andrews, J. Stenger, H. J. Miesner, D. M. Stamper-Kurn, and W. Ketterle, *Nature* **392**, 151 (1998).
- [41] C. Chin, R. Grimm, P. Julienne, and E. Tiesinga, *Rev. Mod. Phys.* **82**, 1225 (2010).
- [42] D. M. Stamper-Kurn, M. R. Andrews, A. P. Chikkatur, S. Inouye, H. J. Miesner, J. Stenger, and W. Ketterle, *Phys. Rev. Lett.* **80**, 2027 (1998).
- [43] L. E. Sadler, J. M. Higbie, S. R. Leslie, M. Vengalattore, and D. M. Stamper-Kurn, *Nature* **443**, 312 (2006).
- [44] H. Strobel, W. Muessel, D. Linnemann, T. Zibold, D. B. Hume, L. Pezzè, A. Smerzi, and M. K. Oberthaler, *Science* **345**, 424 (2014).

- [45] D. S. Hall, M. R. Matthews, J. R. Ensher, C. E. Wieman, and E. A. Cornell, *Phys. Rev. Lett.* **81**, 1539 (1998).
- [46] G. Bornet, G. Emperauger, C. Chen, B. Ye, M. Block, M. Bintz, J. A. Boyd, D. Barredo, T. Comparin, F. Mezzacapo, T. Roscilde, T. Lahaye, N. Y. Yao, and A. Browaeys, *Nature* **621**, 728 (2023).
- [47] D. Katic, and M. Vukobratovic, Springer Science & Business Media **25**, 113 (2013).
- [48] T. Holstein, and H. Primakoff, *Phys. Rev.* **58**, 1098 (1940).
- [49] J. Kennedy, and R. Eberhart, Particle swarm optimization. in: *Proceedings of the 4th IEEE International Conference on Neural Networks* (1995).
- [50] A. Coloni, M. Dorigo, and V. Maniezzo, Distributed Optimization by Ant Colonies, actes de la première conférence européenne sur la vie artificielle. **134**, 142 (1991).
- [51] X. S. Yang, *Nature-inspired metaheuristic algorithms*. Luniver press (2010).

